Diffusive and ballistic motion in superconducting hybrid structures

N. R. Claughton, R. Raimondi, and C. J. Lambert
School of Physics and Chemistry, Lancaster University, Lancaster, LA1 4YB, England
(Received 29 September 1995; revised manuscript received 11 December 1995)

We examine transport properties of superconducting hybrid mesoscopic structures, in both the diffusive and ballistic regimes. For diffusive structures, analytic results from quasiclassical theory are compared with predictions from numerical, multiple-scattering calculations performed on small structures. For many structures, the two methods yield comparable results and in some cases, quantitative agreement is obtained. These results not only demonstrate that quasiclassical theory can yield the ensemble averaged conductance $\langle G\rangle$ of small structures of dimensions of order 10–20 Fermi wavelengths, but also establish that numerical-scattering calculations on such small structures can yield results for $\langle G\rangle$ which are characteristic of much larger systems. One exception arises for Andreev interferometers, where quasiclassical theory predicts a vanishing conductance at a phase difference $\phi=\pi$, whereas our numerical approach yields a finite value. We suggest that this is a consequence of the one-dimensional nature of the currently available quasiclassical descriptions. Having compared the two approaches, we extend the multiple-scattering analysis to the ballistic limit, where the sample dimensions become smaller than the elastic mean free path. In this limit, the numerical results can be understood in terms of a two-channel model, which emphasizes the role of interchannel scattering.

I. INTRODUCTION

When a normal metal (N) makes contact with a superconductor (S), classical tunnelling theory predicts that as a consequence of the existence of a superconducting energy gap, the low-temperature subgap conductance will vanish. Andreev scattering[1] provides an alternative mechanism for charge transport through such an N-S junction and for an ideal interface,[2] leads to a zero-voltage conductance which is almost twice that of the normal state. In the presence of an insulating layer (I), Andreev scattering becomes less effective and in the absence of disorder, the subgap conductance of an N-I-S junction is predicted to be depressed compared with that of the normal state. In contrast, at low enough temperatures, experiments on N-I-S junctions[3] reveal the existence of a zero-voltage conductance peak, with a value comparable to the conductance in the normal state. This effect is due to the interplay between tunneling and disorder-induced scattering and has been observed in experiments involving quantum wells with superconducting electrodes,[4] superconductor-normal metal microjunctions,[5] and superconductor–two-dimensional electron gas (2DEG)–superconductor structures.[6] These have been interpreted using a number of theoretical approaches, including quasiclassical Green-function techniques,[7–12] tunneling Hamiltonian methods,[13,14] multiple-scattering techniques,[15–17] and random-matrix theory.[18,19]

Recently, following a number of theoretical papers on disordered transport in the presence of two superconducting contacts,[20–22] several experiments aimed at probing the phase-coherent nature of Andreev scattering have been carried out. These involve a normal metal in contact with superconductors S_1 and S_2, with order parameter phases ϕ_1, ϕ_2, whose order-parameter phase difference $\phi=\phi_1-\phi_2$ can be controlled by external means. For a diffusive system of size L, with diffusion coefficient D, early theoretical work[20,21] predicted that in the high-temperature limit $T>T^*$, where $k_BT^*=hD/L^2$, the ensemble averaged conductance $\langle G\rangle$ should be a periodic function of ϕ, with fundamental period π, whereas in the low-temperature regime $T<T^*$, it was predicted[22,23] that the fundamental periodicity of $\langle G\rangle$ would be 2π. This prediction of a 2π periodicity is a common feature of all recent theories of $\langle G\rangle$ (Refs. 13, 14, and 24–26) and of recent experiments.[27–31]

Despite much progress, many details of such Andreev interferometers remain to be understood. In particular, there exists no general theory of the amplitude of oscillation, the nature of the zero-phase extremum and the harmonic content of the conductance-phase characteristic. Experiments on various geometries, in different transport regimes have yielded amplitudes of oscillation which differ by many orders of magnitude. It has also been questioned whether analytical theories that mainly apply in the diffusive limit can be used in the quasiballistic case.[30]

One difficulty in establishing a general theory is that most theoretical papers are based on a single technique, with little detailed comparison with the results of other approaches. For example, distinct analytical theories exist for the ballistic, diffusive, and strongly disordered regimes, but there is no analytical theory capable of describing the crossover between them. In contrast, exact numerical solutions of the Bogoliubov-de Gennes equation[32] can easily cross from one regime to another, but are limited to system sizes of order a hundred Fermi wavelengths.

In this paper, we undertake a detailed comparison between an exact numerical, multiple-scattering technique and quasiclassical theory. The former was first used to solve the Bogoliubov-de Gennes equation for disordered, one-dimensional systems[33] and soon after generalized to higher dimensions,[34] while the latter, developed in the context of nonequilibrium superconductivity,[35–38] when supplemented by the appropriate boundary conditions,[39,40] has recently yielded a variety of results for ensemble averaged conductances in the diffusive limit.[7–12] Once agreement between the

two approaches is obtained in the diffusive limit, we then use the numerics to follow the crossover to the ballistic regime, where the electron mean free path becomes comparable with the system size.

The comparison will be carried out by examining two canonical examples of mesoscopic superconducting hybrid structures, namely an *N-I-S* junction and an Andreev interferometer. In Sec. II we briefly recall some results of the quasiclassical Green-function approach for these structures and in Sec. III highlight the main features of the numerical-scattering approach. Whereas a quasiclassical approach yields a one-dimensional theory whose results depend only on the topology of the structure, the numerical calculations, in common with real experiments, require the specification of a suitable geometry. In Sec. IV we present a detailed discussion of the geometry and numerical parameters needed to reproduce the results of quasiclassical theory. Having established agreement between the two approaches we then depart, in Sec. VI from the diffusive limit and investigate the crossover to ballistic transport, which is particularly relevant to the experiments of Ref. 30.

II. RESULTS FROM QUASICLASSICAL THEORY

In this section, we highlight some predictions of the quasiclassical approach of Refs. 7–12. These theories focus on the ensemble averaged conductance $\langle G\rangle$ and ignore the weak localization contribution discussed in Refs. 20 and 21. The latter does not scale with the system size and in systems with a conductance much larger than $2e^2/h$, can be neglected. The results of Refs. 7–12 are obtained by solving the following equation for the quasiclassical Green function $\hat{g}$ in the diffusive limit $D\partial_r(\hat{g}\partial_r\hat{g})+\iota E[\hat{\tau}_z,\hat{g}]=0$, where E is the quasiparticle excitation energy.[41] In what follows, we shall consider only the $E=0$ limit of this equation, which applies to a diffusive system, whose length L is assumed to satisfy the inequalities $L\ll\xi$, where $\xi^2=D/\Delta_0$ and $\xi^2=D/E$, in the superconducting and normal region, respectively. Here D is the diffusion coefficient, Δ_0 the energy gap, and $E=eV$, where V is the applied voltage. Furthermore all temperatures and voltages are assumed to be much smaller than Δ_0. For convenience in what follows, we shall also restrict the analysis to zero temperature.

In units of $2e^2/h$, theory predicts[11,19] that the total conductance G of the structure shown in Fig. 1(a) may be computed from the equation

$$\frac{1}{G}=\frac{1}{G_{\rm diff}}+\frac{1}{G_{\rm tun}\sin\theta}, \tag{1}$$

where θ is a solution of the transcendental equation

$$G_{\rm diff}\theta=G_{\rm tun}\cos\theta \tag{2}$$

and $G_{\rm tun}$, $G_{\rm diff}$ are the respective conductances of the tunnel junction and diffusive region in isolation.

There are two obvious limits to take. The first is where $G_{\rm tun}/G_{\rm diff}\to 0$ for which $\theta\approx G_{\rm tun}/G_{\rm diff}\approx\sin\theta$ and hence

$$\frac{1}{G}\approx\frac{G_{\rm diff}}{G_{\rm tun}^2}. \tag{3}$$

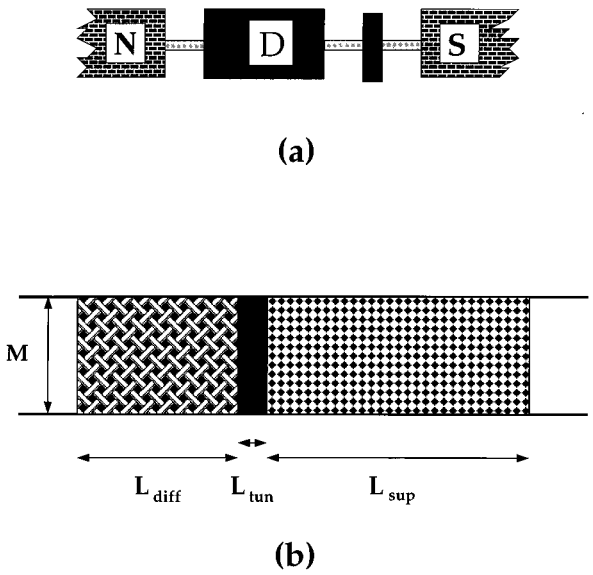

FIG. 1. (a) Schematic picture of an *N-I-S* junction for analysis using circuit theory. (b) Picture of the tight-binding lattice used to model a two-dimensional *N-I-S* structure.

The second limit is $G_{\rm tun}/G_{\rm diff}\to\infty$ in which $\theta\to\pi/2$. This yields

$$\frac{1}{G}\approx\frac{1}{G_{\rm diff}}+\frac{1}{G_{\rm tun}}. \tag{4}$$

Equation (3) has been also directly obtained in the tunneling Hamiltonian limit.[13] Furthermore, as emphasized in Ref. 19, the change of the power in the dependence on the tunnel junction conductance $G_{\rm tun}$, as described by Eqs. (3) and (4), reflects the combined effect of the Andreev scattering at the *N-S* interface and the interference effects in the mesoscopic phase-coherent disordered normal region. In the regime described by Eq. (4) and when $G_{\rm tun}\ll 1$, the conductance of the *N-S* junction appears to be the same as in the normal state and the total resistance is obtained by simply adding up in series the resistances of the diffusive region and tunnel junction. Equations (1) and (2) may be solved numerically to yield the resistance $R_{\rm tot}=1/G$ of the system as a function of $G_{\rm diff}$ and $G_{\rm tun}$. The result of such an exercise for a fixed value $G_{\rm diff}=1.6$ and a variable $G_{\rm tun}$ is shown by curve (a) of Fig. 2. Also plotted are the limits given by Eqs. (3) and (4) represented by the dashed lines (e) and (d). Curve (b) shows the results of the numerical simulation described in Sec. IV.

As a second example, quasiclassical theory predicts[11] that the conductance G of the structure depicted in Fig. 3(a) may be computed from the equation

$$G=\frac{4G_1^2G_2^2\cos^2(\phi/2)}{\{G_1^2+4G_2^2\cos^2(\phi/2)\}^{3/2}}, \tag{5}$$

where G_1 is the conductance of the tunnel junction (1), G_2 is the conductance of the tunnel junction (2) and ϕ is the phase difference between the two superconductors. In the limit $G_1\gg G_2$, this simplifies to the expression

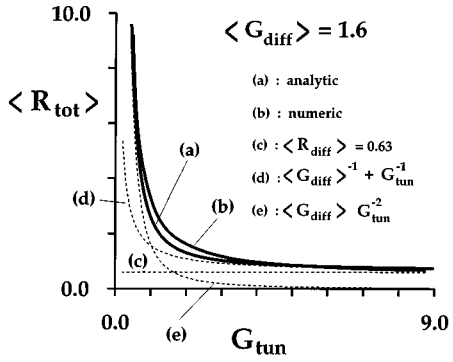

FIG. 2. Conductance of the *N-I-S* structures of Fig. 1, as a function of the conductance G_{tun} of the tunnel junction. The various curves refer to (a) analytic theory; (b) numerical simulation; (c) resistance of the diffusive region $\langle R_{\mathrm{diff}}\rangle = 0.63 = \langle G_{\mathrm{diff}}\rangle^{-1}$; (d) asymptotics at high transparency $G_{\mathrm{tun}} \gg \langle G_{\mathrm{diff}}\rangle$; (e) asymptotics at low transparency $G_{\mathrm{tun}} \ll \langle G_{\mathrm{diff}}\rangle$.

$$G = 4\frac{G_2^2}{G_1}\cos^2(\phi/2), \tag{6}$$

whereas if $G_2 \gg G_1$ then

$$G = \frac{1}{2}\frac{G_1^2}{G_2}\frac{1}{|\cos(\phi/2)|}. \tag{7}$$

Figure 4 shows four plots of Eq. (5) for each combination of $G_1 = 0.2, 2.0$ and $G_2 = 0.2, 2.0$. One can see that for $G_1 = G_2$ there is a zero-phase minimum, as there is for $G_1 \ll G_2$. When $G_1 \gg G_2$ however, one finds a zero-phase maximum. In all cases the conductance vanishes when the phase difference between the superconductors is π. Corresponding analytical results have been obtained for ballistic interferometers in one[42,43] and two[44] dimensions.

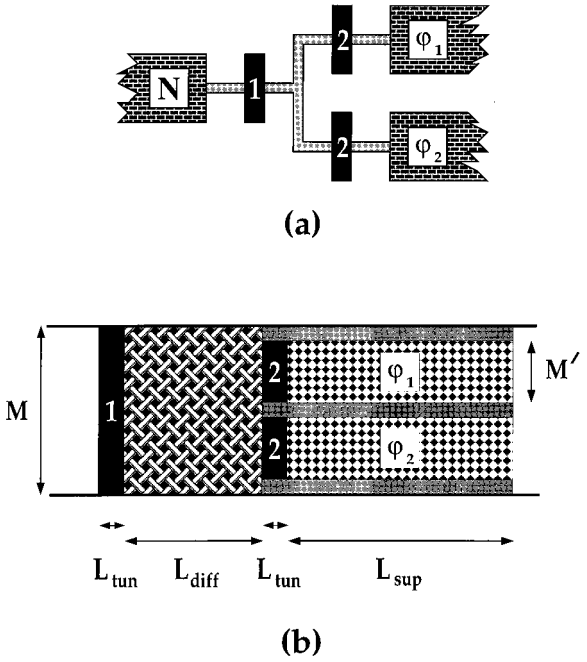

FIG. 3. (a) Schematic picture of an interferometer analyzed using circuit theory. (b) Picture of an interferometer formed from a two-dimensional tight-binding lattice.

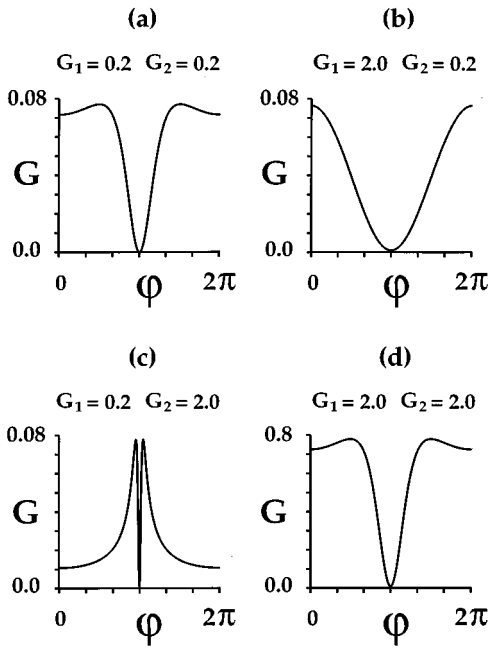

FIG. 4. Analytic results for the conductance versus phase in the diffusive limit: (a) $G_1 = 0.2$ and $G_2 = 0.2$. (b) $G_1 = 2.0$ and $G_2 = 0.2$. (c) $G_1 = 0.2$ and $G_2 = 2.0$. (d) $G_1 = 2.0$ and $G_2 = 2.0$.

III. A SCATTERING APPROACH TO TRANSPORT IN MESOSCOPIC SUPERCONDUCTORS

During the past six years[32–34] we have developed numerical codes capable of yielding exact solutions of the Bogoliubov-de Gennes equation for disordered structures in arbitrary dimensions. Currently there are two independent sets of codes available at Lancaster; one of these is based on a transfer-matrix approach and the other is based on a recursive Green's-function method. Typically these are used as independent crosschecks and therefore there can be no doubt about the accuracy of the results obtained for a given structure. For a two-dimensional system of width less than a few hundred Fermi wavelengths, or for a three-dimensional system of width less than a few tens of Fermi wavelengths, the problem of computing dc transport properties of a phase-coherent system described by mean-field BCS theory is therefore no longer an issue. Just as the appearance of pocket calculators rendered approximate tables for computing elementary functions redundant, the existence of these codes has, for several years, allowed transport properties of small structures to be calculated without further approximation. For larger systems, the key issue is how to extrapolate the results of such calculations to larger numbers of channels. By making contact with quasiclassical theory, the results which follow establish that for many systems, the ensemble averaged conductance obtained from small systems exhibits the essential features of much larger structures.

The numerical codes yield the quantum-mechanical scattering matrix of a given phase-coherent structure and from this the matrix elements $a_{ij} = \partial I_i / \partial(\mu_j - \mu)$, where I_i is the current supplied by a normal reservoir of chemical potential

μ_i and μ is the condensate chemical potential. This approach has been used to evaluate multichannel scattering formulas for the dc electrical conductance[15,32] and more recently thermoelectric properties.[45] In what follows, we focus on hybrid structures connected to normal external reservoirs only. For example for a structure connected to two such reservoirs, the zero-temperature, zero-bias electrical conductance can be written[15,32] (in units of $2e^2/h$),

$$G = T_0 + T_a + \frac{2(R_a R_a' - T_a T_a')}{R_a + R_a' + T_a + T_a'}. \tag{8}$$

In this expression, R_0, T_0 (R_a, T_a) are the coefficients for normal (Andreev) reflection and transmission for zero-energy quasiparticles from reservoir 1, while R_0', T_0' (R_a', T_a') are the corresponding coefficients for quasiparticles from reservoir 2. If each of the external leads connecting the reservoirs to the scatterer contains N open channels, these satisfy $R_0 + T_0 + R_a + T_a = R_0' + T_0' + R_a' + T_a' = N$ and $T_0 + T_a = T_0' + T_a'$. Furthermore, in the absence of a magnetic field, all reflection coefficients are even functions of ϕ, while the transmission coefficients satisfy $T_0'(\phi) = T_0(-\phi)$, $T_a'(\phi) = T_a(-\phi)$. Consequently on quite general grounds, in the absence of a magnetic field, G is predicted to be an even function of ϕ. In the absence of quasiparticle transmission between the two external probes, Eq. (8) reduces to

$$G^{-1} = (2R_a)^{-1} + (2R_a')^{-1}, \tag{9}$$

where $2R_a$ $(2R_a')$ are left (right) boundary conductances, introduced by Blonder, Tinkham, and Klapwijk (BTK).[2]

The numerical codes compute the scattering coefficients of a tight-binding lattice, described by a Bogoliubov-de Gennes Hamiltonian of the form

$$H = \begin{pmatrix} H_0 & \Delta \\ \Delta^* & -H_0^* \end{pmatrix}. \tag{10}$$

If an index n is used to label sites on the lattice and any internal spin degrees of freedom, then H_0 is of the form

$$H_0 = \sum_n \epsilon_n |n\rangle\langle n| + \sum_{(n,m)} V_{n,m} |n\rangle\langle m|. \tag{11}$$

To model a given physical structure, it is necessary to specify certain phenomenological parameters which capture the essential physics. As an example, in the absence of spin-orbit scattering, spin degrees of freedom can be ignored and in the absence of a magnetic field, one chooses $V_{n,m} = -\gamma$ for nearest-neighbor pairs (n,m). If (n,m) are not nearest neighbors, then $V_{n,m} = 0$. In a region free from disorder, the diagonal elements ϵ_n are set equal to a constant ϵ_0, whereas in a disordered region, ϵ_n is a random number uniformly distributed between $\epsilon_0 - W$ and $\epsilon_0 + W$. In the presence of spin singlet, local s-wave pairing, Δ is a diagonal order-parameter matrix with elements Δ_n. In a normal region, $\Delta_n = 0$, whereas in a clean superconducting region, $|\Delta_n|$ is set to a constant value Δ_0. The phase of Δ_n is chosen to equal a value assigned to the superconducting region to which site n belongs. In what follows, the energy scale will be fixed by making the choice $\gamma = 1$.

Of course, the above parameters are not directly accessible experimentally and are not an explicit feature of quasiclassical theory. Therefore when making comparisons, some effort is needed to map one analysis onto another. In d dimensions, for a clean system on a square or cubic lattice, the chemical potential relative to the band bottom is $\mu = \epsilon_0 + 2d\gamma$, the band width is $4d\gamma$ and the effective mass for excitations near the band bottom is $m^* = \hbar^2/(2\gamma a^2)$, where a is the lattice constant. A key parameter in the problem is the dimensionless ratio $\Delta = \Delta_0/\mu$, which takes a value 10^{-3} for conventional low-T_c superconductors such as niobium, but can be as large as 0.1 for high-temperature superconductors, or for a 2DEG in contact with a conventional superconductor. Andreev's approximation, which underpins many analytic theories, including quasiclassical and random-matrix descriptions, is valid only when this parameter is much less than unity.

Other parameters which are needed when making comparisons are the Thouless energy E^*, which for a diffusive structure of width M, length $L_{\rm diff}$ and normal-state conductance G, is given by

$$E^* = hD/L_{\rm diff}^2 = (h/2e^2)G/[n(0)L_{\rm diff}M^{d-1}],$$

where $n(0)$ is the density of states per site. A second parameter is the normal-state, elastic mean free path l, which for a diffusive sample connected to external lead with N open channels, is given by $G = (2e^2/h)Nl/L_{\rm diff}$. Within a numerical simulation on a given geometry, once the model parameters W, γ, ϵ_0, and Δ_0 are chosen, the parameters G, l, $n(0)$, and E^* are computed explicitly.

IV. NUMERICAL RESULTS FOR A *N-I-S* STRUCTURE

In this section, we present a comparison between the predictions of quasiclassical theory and the above numerical-scattering approach, for an *N-I-S* structure. Our aim is to highlight the steps required to obtain a suitable choice of parameters, from which a meaningful comparison can be made. In the literature, numerical results in two dimensions have been obtained by first solving for the scattering matrix of a normal diffusive structure, with or without a tunnel junction and then employing Andreev's approximation to model the Andreev scattering induced by a nearby superconductor.[17] As noted above, this approximation requires that Δ_0 be small compared with the Fermi energy and that there be no disorder in the superconductor. Furthermore for a clean system, Andreev's approximation can yield incorrect results, because even at a clean *N-S* interface, the approximation breaks down[46] when scattering channels are almost closed. For these reasons a comparison with an exact solution of the Bogoliubov-de Gennes equation allows one to examine changes occurring away from the Andreev limit, in a region of parameter space which is more relevant to high-temperature superconductors.

The system to be examined is shown in Fig. 1(b) and consists of a disordered region in contact with a tunnel junction, which is in turn adjacent to a superconducting probe. The simulated structure consists of a two-dimensional tight-binding lattice of width M sites. The disordered region is of length $L_{\rm diff}$ sites, the tunnel junction is $L_{\rm tun}$ sites long and the superconductor has a length $L_{\rm sup}$. In units of $2e^2/h$, the con-

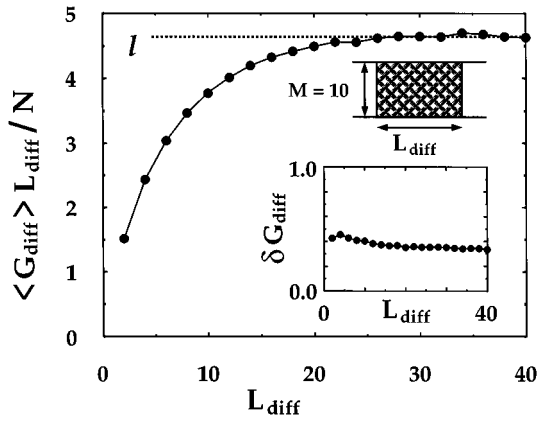

FIG. 5. $\langle G_{\mathrm{diff}}\rangle L_{\mathrm{diff}}/N$ versus L_{diff}. The plateau region signifies the diffusive regime. Here the number of open channels is $N=9$. In the inset standard deviation is also shown.

ductance of a particular realization of the structure will be denoted G and the ensemble-averaged conductance will be written $\langle G\rangle$. In order to make a comparison with quasiclassical theory, it is necessary that the properties of the two resistive components and the superconducting probe be compatible with the assumptions made by the theory.

To identify a suitable choice of parameters, consider first a normal diffusive portion of length L_{diff} and width M, connected to crystalline leads. In units of $2e^2/h$, the conductance of a particular realization of this structure will be denoted G_{diff} and the ensemble-averaged conductance will be written $\langle G_{\mathrm{diff}}\rangle$. The conductance of a diffusive material is inversely proportional to its length and therefore a plot of $\langle G_{\mathrm{diff}}\rangle L_{\mathrm{diff}}$ as a function of L_{diff} will exhibit a plateau in the diffusive regime, with a mean free path given by $l=\langle G_{\mathrm{diff}}\rangle L_{\mathrm{diff}}/N$.

For a sample of width $M=10$, Fig. 5 shows a plot of $\langle G_{\mathrm{diff}}\rangle L_{\mathrm{diff}}/N$ versus L_{diff}. This structure has periodic boundary conditions in the direction tranverse to the current flow and the choice $\epsilon_0=0.2$ was made, which yields $N=9$. Results are shown for a disorder of $W=1$. The length L_{diff} of the disordered region was incremented in steps of two sites from $L_{\mathrm{diff}}=2$ to 40. For each value of L_{diff}, 2000 realizations of disorder were chosen and the conductance G_{diff} computed for each. Then the ensemble average $\langle G_{\mathrm{diff}}\rangle$ and the standard deviation δG_{diff} were calculated.

Figure 5 shows that in the interval $20<L_{\mathrm{diff}}<40$ the system exhibits diffusive behavior, with a mean free path of $l\approx 4.6$. For smaller values of L_{diff}, the system is in the ballistic regime and for larger values, the onset of localization causes the curve to fall. A diffusive system is one for which $l\ll L_{\mathrm{diff}}$ and $l\ll M$. Furthermore if weak localization corrections are to be neglected, we require $Nl\gg L_{\mathrm{diff}}$. For these reasons a judicious choice of length yielding a diffusive system whilst minimizing CPU time is $L_{\mathrm{diff}}=25$. Such a system has an average conductance $\langle G_{\mathrm{diff}}\rangle=1.6$.

To compare with quasiclassical theory, a knowledge of the conductance of the isolated tunnel junction G_{tun} as a function of the barrier height ϵ_b is also required. In what follows, we consider a clean tunnel junction of dimensions $M=10$ and $L_{\mathrm{tun}}=1$, obtained by setting the diagonal elements ϵ_n of all barrier sites n equal to $\epsilon_0+\epsilon_b$. For an isolated barrier connected to crystalline leads of width 10, Fig. 6 shows a plot of

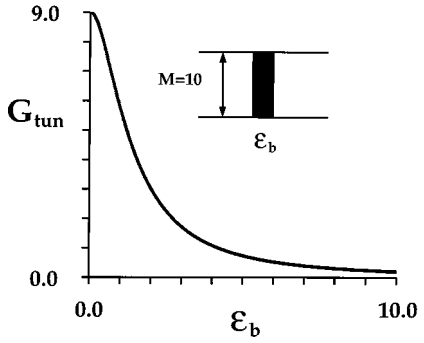

FIG. 6. Conductance G_{tun} of the tunnel junction as a function of the barrier height ϵ_b.

G_{tun} as a function of ϵ_b. To obtain this plot, the conductance G_{tun} is computed for 1000 successive values of the barrier height ϵ_b in the range $0.0<\epsilon_b<10.0$. This choice of barrier heights yields a spread of barrier conductances in the convenient range $0.0<G_{\mathrm{tun}}<9.0$.

Finally, before a comparison with theory can be made, the properties of the superconductor must be chosen such that there be no transmission through the superconducting region and that Andreev's approximation of neglecting normal reflection at the N-S interface is valid. To avoid quasiparticle transmission, it is necessary to choose $L_{\mathrm{sup}}>\xi$, where $\xi=\mu/\Delta_0$ and to minimize normal reflection it is necessary that $\xi\gg 1$. For $\Delta_0=0.05$ and $\epsilon_0=0.2$ the superconducting coherence length is $\xi=76$ and it is found that transmission is negligible for $L_{\mathrm{sup}}>100$. For the above choice of parameters, one finds for the normal and Andreev reflection and transmission coefficients: $R_0=0.064\,85$, $R_a=8.847\,62$, $T_0=0.087\,48$, and $T_a=0.000\,05$.

It should be noted that the condition $\xi\gg 1$ is not sufficient to completely exclude normal reflection at an N-S interface. It is also necessary that ϵ_0 be chosen such that the number of open channels in the external leads is not sensitive to small changes in ϵ_0. This feature is illustrated in Fig. 7, which shows as a function of ϵ_0, the conductance of a clean superconducting region of width $M=50$ and length $L_{\mathrm{sup}}=5$, attached to crystalline normal leads. Results are shown for five values of Δ_0: $\Delta_0=0$, 10^{-2}, 10^{-1}, 0.3, and 0.5. For $\Delta_0=0$, the conductance is equal to the number of open channels and changes by unity whenever an external quasiparticle channel closes. At these values of ϵ_0, switching on an infinitesimal Δ_0 causes the conductance to decrease by unity. As shown in the figure, finite values of Δ_0 smear the conductance steps and

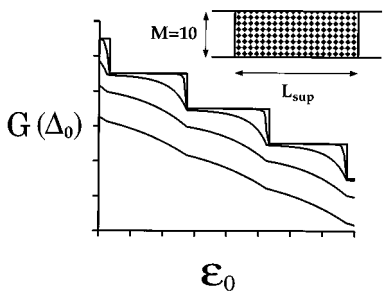

FIG. 7. The conductance $G(\Delta_0)$ of a clean superconducting region of length $L_{\mathrm{sup}}=5$, width $M=50$, plotted as a function of the site energy ϵ_0, for 5 different values of Δ_0.

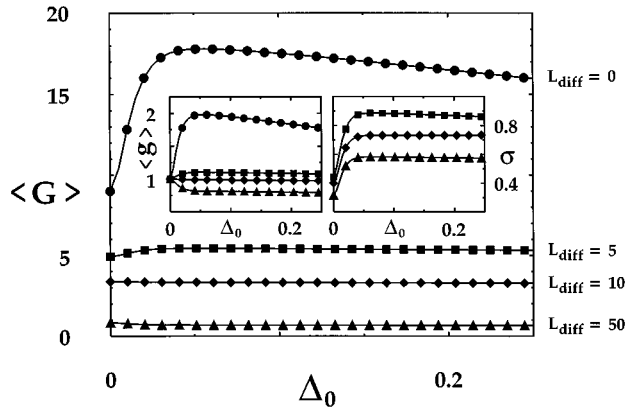

FIG. 8. Plots of the mean conductance $\langle G(\Delta_0)\rangle = N - R_0 + R_a$ as a function of Δ_0, for a diffusive conductor of width $M=10$ and four different lengths. The left inset shows the conductance $\langle g\rangle = \langle G(\Delta_0)\rangle / \langle G(0)\rangle$, scaled by the normal-state conductance. The right inset shows the rms deviation $\sigma = \langle (G(\Delta_0) - \langle G(\Delta_0)\rangle)^2\rangle^{1/2}$.

suppress the conductance. Both of these features lie outside Andreev's approximation.[46] To achieve compatibility with the assumptions of circuit theory, the choice $\epsilon_0 = 0.2$ was made, which places a system of width 10 between two conductance steps and avoids the above sensitivity to changes in Δ_0.

Having identified a choice of parameters which is compatible with quasiclassical theory, numerical results for the combined structure of Fig. 1(b) can now be obtained. To summarize, this structure has the following properties: width $M=10$, number of open channels $N=9$, band filling factor $\epsilon_0=0.2$ leading to a chemical potential $\mu=3.8$, length of tunnel junction $L_{\rm tun}=1$, barrier heights $0.0<\epsilon_b<10.0$, barrier conductances $0.0<G_{\rm tun}<9.0$, length of diffusive region $L_{\rm diff}=25$, diffusive disorder width $W=1$, conductance of diffusive region $\langle G_{\rm diff}\rangle = 1.6$, length of superconductor $L_{\rm sup}=100$, superconducting coherence length $\xi=76$, superconducting order parameter $\Delta_0=0.05$, elastic mean free path $l \approx 4.5$.

First consider the case of no barrier, where $\epsilon_b=0$. In this case, quasiclassical theory insists that the conductance of a diffusive region in contact with a superconductor should be identical with the normal-state conductance of the diffusive region. Figure 8 shows plots of the mean conductance $\langle G\rangle = N - R_0(\Delta_0) + R_a(\Delta_0)$ as a function of Δ_0, for disordered regions of four different lengths. In the normal state ($\Delta_0=0$) $\langle G\rangle$ reduces to $T_0(0) = N - R_0(0)$ and in the presence of a sufficiently long superconductor, to the BTK conductance $2R_a(\Delta_0)$. The left insert shows the quantity $\langle g\rangle = \langle N - R_0(\Delta_0) + R_a(\Delta_0)\rangle / \langle T_0(0)\rangle$ (i.e., the conductance divided by the normal-state conductance). The right insert shows the root-mean-square deviation $\sigma = \langle [G(\Delta_0) - \langle G(\Delta_0)\rangle]^2\rangle^{1/2}$. These show that in the ballistic limit $L_{\rm diff}=0$, the conductance rises to a value almost double that of the normal state, before decreasing with increasing Δ_0. In contrast, the mean conductance of a diffusive normal region is relatively insensitive to the onset of superconductivity, with the largest relative change corresponding to the largest value of $L_{\rm diff}$, (i.e., the smallest value of the normal-state conductance). It should be noted however that even though the mean is insensitive to Δ_0, the fact that the rms deviation σ is nonzero reveals that for individual samples, large changes of arbitrary sign can occur.

Having examined a diffusive conductor with no barrier, we now turn to the case of finite ϵ_b. Curve (b) of Fig. 2 shows numerical results in the presence of a tunnel barrier. For 50 equally spaced barrier heights in the range $0.0<\epsilon_b<10.0$, 500 realizations of disorder in the diffusive region were selected and the total conductance G computed for each realization. The ensemble-averaged conductance $\langle G\rangle$ was then calculated and finally the total resistance $\langle R_{\rm tot}\rangle = 1/\langle G\rangle$ plotted against the computed conductance $G_{\rm tun}$ of the isolated tunnel junction. Since the average conductance of the diffusive region $\langle G_{\rm diff}\rangle$ is also known, Eq. (1) can be evaluated to yield the corresponding analytical result, curve (a) of Fig. 2. This demonstrates that in the range of validity of quasiclassical theory, quantitative agreement with the numerical-scattering approach is obtained.

V. NUMERICAL RESULTS FOR ANDREEV INTERFEROMETERS

Having examined a simple N-I-S structure, we now compare numerical results for the tight-binding structure of Fig. 3(b), with the predictions of quasiclassical theory for the one-dimensional (1D) system of Fig. 3(a). The latter comprises a tunnel junction connected by diffusive 1D wires to a fork. Each of the two arms of the fork is a diffusive wire, connected via tunnel junctions to infinitely long superconductors. The conductance of the diffusive wires is assumed to be much greater than that of the tunnel junctions.

The two-dimensional tight-binding realization of this structure is shown in Fig. 3(b), which consists of a tunnel junction (1) lying next to a diffusive region which is in turn adjacent to two superconductors. The superconductors are separated from each other by an insulating layer and from the diffusive region by two identical tunnel junctions (2). The superconductors $i=1,2$ have order parameter phases ϕ_i, but are identical in every other respect. In order that they may successfully represent superconducting probes of infinite length, they are chosen in such a way that quasiparticle transmission through them is negligible.

The diffusive region is of length $L_{\rm diff}$ sites, each tunnel junction is $L_{\rm tun}$ sites long and the superconductors have a length $L_{\rm sup}$. To model a superconducting reservoir, $L_{\rm sup}$ is again chosen sufficiently large such that there is negligible transmission through the superconductor. The system width and the width of both the diffusive region and the tunnel junction (1) is M sites. On the right of the diffusive region, the three insulating layers are each one site thick and therefore the superconductors are each of width M' (where $2M' = M - 3$).

In the simulation, the conductances G_1 and G_2 of the tunnel junctions are fixed at values which replicate the three situations of Fig. 4, namely $G_1 = G_2$, $G_1 \ll G_2$, and $G_1 \gg G_2$ to enable comparisons to be made with the analytic results. In each case, the phase difference between the two superconductors is varied and the total conductance G plotted as a function of phase for a particular realization of disorder in the diffusive region. Ensemble averaging over many disorder realizations yields the conductance $\langle G\rangle$ which is independent

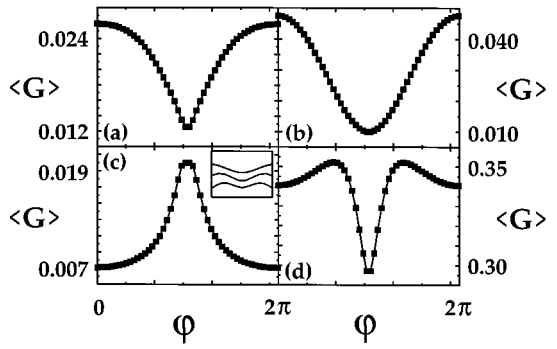

FIG. 9. Numerical results for the conductance versus phase for $L_{\mathrm{diff}}=10$: (a) $G_1=0.2$ and $G_2=0.2$. (b) $G_1=2.0$ and $G_2=0.2$. (c) $G_1=0.2$ and $G_2=2.0$. (d) $G_1=2.0$ and $G_2=2.0$.

of the microscopic configuration of the system and may be usefully compared with the results of Eq. (5) (see below) and Fig. 4.

In what follows, we examine a sample of width $M=15$, with a diagonal matrix element $\epsilon_0=0.2$ and periodic boundary conditions, for which the number of open channels is $N=13$. The disorder is chosen to be $W=1$ and again from a graph of the form of Fig. 5, we obtain a mean free path of $l\approx 4.9$. In most cases of experimental interest, the conductance of the diffusive ''wires'' may be considered to be much greater than that of the tunnel junctions. In order to take into account this situation in our numerical simulations, one has to put some restrictions on the length of the diffusive region, since the conductance decreases with length. A compromise must therefore be found between the desire to increase the length into the diffusive regime and the wish to decrease it in order to maintain a high conductance. In what follows a choice $L_{\mathrm{diff}}=10$ is made, for which $\langle G_{\mathrm{diff}}\rangle\approx 5.1$.

To create a tunnel barrier of length $L_{\mathrm{tun}}=1$ and width M, all diagonal elements ϵ_i of sites within the barrier were set to a value $\epsilon_i=\epsilon_0+\epsilon_b$. For an isolated tunnel junction (1) of width $M=15$, the values $\epsilon_b=3.52$, 12.27 yield, respectively, the conductances $G_1=2.0$, 0.2 and for an isolated tunnel junction (2) of width $M'=6$, the values $\epsilon_b=1.87$, 7.75 yield conductances $G_2=2.0$, 0.2. These values of ϵ_b were used in the simulations of Fig. 9. As in the previous section, the choice $\epsilon_0=0.2$, $\Delta_0=0.05$, $L_{\mathrm{sup}}=100$ was made. For the superconductor alone, connected to crystalline normal leads of width $M'=6$, the values of the normal and Andreev reflection and transmission coefficients were found to be: $R_0=0.02155$, $R_a=4.92905$, $T_0=0.04937$, $T_a=0.00003$. For such a structure, there are five open channels and as a consequence, the sum of these four coefficients is 5. Finally, in order to model an insulating barrier, the diagonal matrix elements ϵ_i referring to a site i on the barrier between the superconductors, were each set to the large number $\epsilon_i=\epsilon_0+50$.

By combining the above components to yield the complete structure of Fig. 3(b), one obtains the structure to be analyzed numerically, whose parameters are as follows: total width $M=15$, superconductor width $M'=6$, number of open channels in normal lead $N=13$, band filling $\epsilon_0=0.2$, chemical potential $\mu=3.8$, length of tunnel junctions $L_{\mathrm{tun}}=1$, length of diffusive region $L_{\mathrm{diff}}=10$, disorder width $W=1.0$, conductance of diffusive region $\langle G_{\mathrm{diff}}\rangle=5.1$, length of superconductor $L_{\mathrm{sup}}=100$, superconducting coherence length $\xi=76$, superconducting order parameter $\Delta_0=0.05$.

To carry out the simulation, the conductances G_1 of tunnel junction (1) and G_2 of tunnel junction (2) were fixed and a particular realization $\{\epsilon_i\}$ of disorder in the diffusive region was selected. Then the phase difference $\phi=\phi_1-\phi_2$ between superconductors 1 and 2 was varied from zero to 2π. This was done by fixing $\phi_1=0$ and choosing 50 evenly spaced values of ϕ_2. For each value of ϕ, 200 different diffusive regions were obtained and the conductance G of the whole system computed for each. The ensemble-averaged conductance $\langle G\rangle$ was then calculated. The graphs of Fig. 9 show plots of $\langle G\rangle$ as a function of the phase difference ϕ for the following four combinations of G_1 and G_2. They are (a) $G_1=0.2$ $G_2=0.2$, (b) $G_1=2.0$ $G_2=0.2$, (c) $G_1=0.2$ $G_2=2.0$, (d) $G_1=2.0$ $G_2=2.0$.

Apart from the different vertical scales, the numerical results of Fig. 9 and the analytic results of Fig. 4 share many qualitative features and also exhibit some interesting differences. Figure 9(d) is comparable with 4(d); each exhibits a zero-phase minimum and a further minimum at $\phi=\pi$. Similarly 9(b) is comparable with 4(b); each exhibits a zero-phase maximum, with a minimum at $\phi=\pi$. The remaining curves compare less favorably. Whereas the analytic results of Figs. 4(a) and 4(d) are necessarily identical, there is no such restriction on the numerics and as shown in Fig. 9(a), decreasing the conductances G_1 and G_2 can produce qualitative changes. As a consequence, Fig. 9(a) possesses a zero-phase maximum, whereas Fig. 4(a) possesses a zero-phase minimum.

Figures 4(c) and 9(c) also reveal some differences. Each possesses a zero-phase minimum, but at $\phi=\pi$, where the analytic result vanishes, the numerical result is almost maximal. The inset in Fig. 9(c) shows a ''blow up'' of the region $\pi-0.15\leqslant\phi\leqslant\pi+0.15$, with $G_1=0.2$ and $G_2=2.0$. The inset shows three curves, obtained by averaging over different numbers of samples, namely 200, 1000, and 2000 realizations of the disorder. These demonstrate that in contrast with Eq. (5), the numerical results 9(c) possess a shallow, local minimum at $\phi=\pi$. This discrepancy is not just an artifact of the numerical calculations. We will see below that this is a consequence of the actual two-dimensional nature in the system considered, whereas quasiclassical theory is effectively a one-dimensional theory.

Finally, we end this discussion by noting that for systems with a small number of open channels, the behavior of an individual sample can be very different from that of the mean. For each of the four cases (a) to (d), Fig. 10 shows each of the 200 plots of conductance G from which the ensemble averages of Fig. 9 were calculated. Apart from the case 10(b), where individual members of the ensemble behave in the same manner as the average, the nature of the extrema at $\phi=0$, π depends on the microscopic realization of the disorder. We also note that by changing the dimensions of the sample, one can change the details of Fig. 9, but not the qualitative shape. For example by increasing the length L_{diff} from 10 to 15, the local minimum at $\phi=\pi$ in Fig. 9(c) becomes more pronounced, but further increasing L_{diff} to 20 causes the minimum to become more shallow.

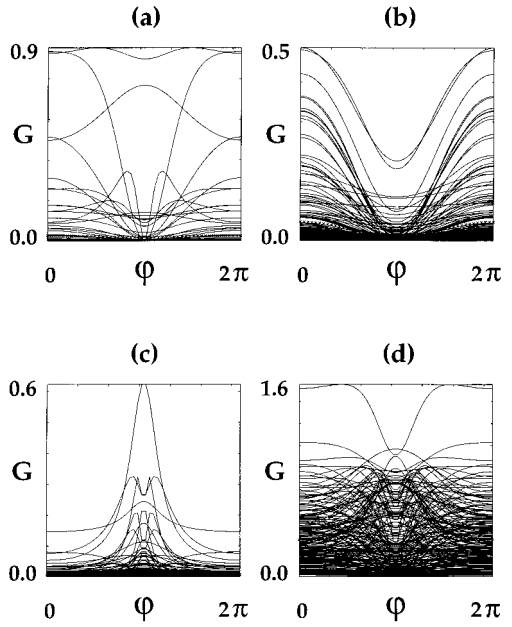

FIG. 10. Numerical results for the conductance versus phase for individual realizations of the disorder: (a) $G_1=0.2$ and $G_2=0.2$. (b) $G_1=2.0$ and $G_2=0.2$. (c) $G_1=0.2$ and $G_2=2.0$. (d) $G_1=2.0$ and $G_2=2.0$.

VI. DESCRIPTION OF THE BALLISTIC LIMIT: TWO-CHANNEL MODEL

Having compared the quasiclassical theory of Refs. 7–12 with the numerical-scattering approach in the diffusive limit, we now examine the crossover to the ballistic regime, where the former is inapplicable. This discussion will demonstrate why a two-dimensional theory predicts a finite conductance at $\phi=\pi$, whereas a one-dimensional, quasiclassical theory yields $G(\pi)=0$. We initially focus attention on the interferometer of Fig. 3(b) and examine the change in behavior as the length $L_{\rm diff}$ of the diffusive region becomes smaller than the elastic scattering length l. Apart from the change in $L_{\rm diff}$, all other parameters are fixed to the values used in Fig. 9. Figure 11 shows results for a diffusive region of length $L_{\rm diff}=5$ and Fig. 12 for a length $L_{\rm diff}=1$. For this geometry, apart from an increase in the amplitude of oscillation, the qualitative shape of the curves is unchanged and therefore an understanding of the ballistic limit will also provide insight

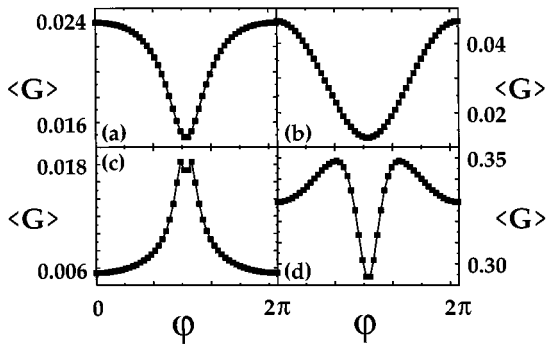

FIG. 11. Numerical results for the conductance versus phase for $L_{\rm diff}=5$: (a) $G_1=0.2$ and $G_2=0.2$. (b) $G_1=2.0$ and $G_2=0.2$. (c) $G_1=0.2$ and $G_2=2.0$. (d) $G_1=2.0$ and $G_2=2.0$.

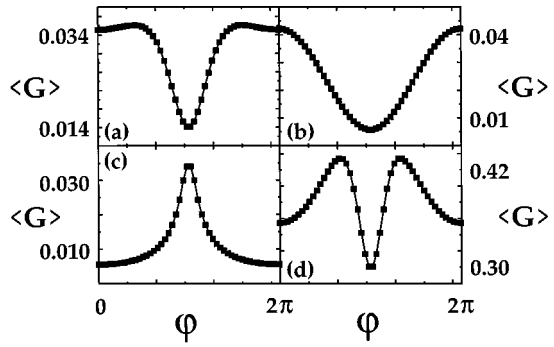

FIG. 12. Numerical results for the conductance versus phase for $L_{\rm diff}=1$: (a) $G_1=0.2$ and $G_2=0.2$. (b) $G_1=2.0$ and $G_2=0.2$. (c) $G_1=0.2$ and $G_2=2.0$. (d) $G_1=2.0$ and $G_2=2.0$.

into the behavior of the conductance of the diffusive structure at $\phi=\pi$.

To obtain such an understanding we now develop an analytic theory of the ballistic limit, based on a multiple-scattering description of a clean N-S interface. Consider, for example, the structure of Fig. 3(b). In the absence of disorder, and when there is no phase difference between the two superconductors, translational invariance in the direction transverse to the current flow allows one to reduce the two-dimensional system to the sum over many independent one-dimensional channels. When a phase difference between the superconductors is imposed, interchannel coupling is introduced, but as shown below this coupling typically involves only pairs of channels, in such a way that an accurate description is obtained by summing over independent *pairs* of coupled channels. The theory developed below is based on a two-channel description of the left-hand boundary conductance [cf. Eq. (9)]

$$G_B(\phi)=2R_a=2\,\mathrm{Tr}r_a r_a^{\dagger}=\sum_{i,j=1}^{N}(R_a)_{ij}, \tag{12}$$

where $(R_a)_{ij}=|(r_a)_{ij}|^2$ is the Andreev reflection probability from channel j to channel i. The Andreev reflection coefficient is of the form $R_a=R_{\rm diag}+R_{\text{off-diag}}$ where $R_{\rm diag}=\Sigma_{i=1}^{N}(R_a)_{ii}$ and $R_{\text{off-diag}}$ is the remaining contribution from interchannel scattering, $R_{\text{off-diag}}=\Sigma_{i\neq j=1}^{N}(R_a)_{ij}$. If channels only couple in pairs, both the off-diagonal scattering and the diagonal scattering will scale as the number of channels.

In the absence of disorder, the structure of Fig. 3(b) may be reduced to a simpler one in which a normal barrier only is placed in front of the two superconductors. This is because the motion between the two barriers of Fig. 3(b) is now ballistic and can easily be taken into account by trivial phase factors. The two barriers can then be reduced to one effective barrier only. Consider now a normal barrier to the left of a N-S interface. Particles (holes) impinging on the normal scatterer are described by a scattering matrix s_{pp}, (s_{hh}), and those arriving at the N-S interface by a reflection matrix ρ, where

$$s_{pp}=\begin{pmatrix} r_{pp} & t'_{pp} \\ t_{pp} & r'_{pp} \end{pmatrix}, \quad \rho=\begin{pmatrix} \rho_{pp} & \rho_{ph} \\ \rho_{hp} & \rho_{hh} \end{pmatrix}.$$

The elements of s and ρ are themselves matrices describing scattering between open channels of the external leads. For an ideal interface, where Andreev's approximation is valid, ρ_{pp} and ρ_{hh} are negligible and in what follows will be set to zero. As a consequence, ρ_{hp} and ρ_{ph} are unitary and one obtains[16] $r_a = t'_{hh} M^{-1}_{pp} t_{pp}$, with $M_{pp} = 1 - r'_{pp}\rho_{ph} r'_{hh}\rho_{hp}$. In contrast with the analysis of Ref. 16, where ρ_{hp} is proportional to the unit matrix, the interference effect of interest here is contained in the fact that ρ_{hp} induces off-diagonal scattering. Substituting r_a into Eq. (12) and taking advantage of particle-hole symmetry at $E=0$, yields

$$G = 2\,\mathrm{Tr}(TQ^{-1}T(Q^{\dagger})^{-1}) \tag{13}$$

where $Q = \rho^{t}_{ph} + (r')_{pp}\rho_{ph}(r')^{\dagger}_{pp}$, with $T = t_{pp}t^{\dagger}_{pp}$ the transmission matrix of the normal scattering region. This multiple-scattering formula for the boundary conductance is valid in the presence of an arbitrary number of channels and in any dimension.

Equation (13) is very general and makes no assumption about the nature of matrices ρ_{ph} and s_{pp}. We now introduce a two-channel model in which ρ_{ph} is chosen to be an arbitrary two-dimensional unitary matrix. In the absence of disorder, t_{pp} and r_{pp} are diagonal and therefore the only interchannel coupling is provided by ρ_{ph}. Substituting these matrices into Eq. (13), yields an expression for r_a involving a single phase θ, whose value is a linear combination of phase shifts due to normal reflection at the barrier, Andreev reflection at the N-S interface and the phase accumulated by an excitation traveling from the barrier to the interface. The result for the sum of the two diagonal elements is

$$R_{\mathrm{dia}}(\phi,\theta) = (R_a)_{11} + (R_a)_{22} = \frac{cA}{[cC + s(D - E\,\cos\theta)]^2} \tag{14}$$

and for the sum of the two off-diagonal elements

$$R_{\text{off-diag}}(\phi,\theta) = (R_a)_{12} + (R_a)_{21} = \frac{sB(D - E\,\cos\theta)}{[cC + s(D - E\,\cos\theta)]^2}, \tag{15}$$

where $A = T_1^2(1+R_2)^2 + T_2^2(1+R_1)^2$, $B = 2T_1T_2$, $C = (1+R_1)(1+R_2)$, $D = 1 + R_1R_2$, $E = 2\sqrt{R_1R_2}$, $R_1 = 1 - T_1$, $R_2 = 1 - T_2$, $c = \cos^2\phi/2$, and $s = \sin^2\phi/2$. After averaging over the rapidly varying phase θ, this yields

$$R_{\mathrm{dia}}(\phi) = cA\,\frac{cC + sD}{[(cC + sD)^2 - s^2E^2]^{3/2}}$$

and

$$R_{\text{off-diag}}(\phi) = sB\,\frac{cCD + s(D^2 - E^2)}{[(cC + sD)^2 - s^2E^2]^{3/2}}. \tag{16}$$

For a given value of ϕ, once the normal barrier transmission coefficients T_1 and T_2 of the two channels are chosen, the right-hand sides of Eqs. (16) are completely determined.

We now compare the analytic results of Eq. (16) for $R_{\mathrm{dia}}(\phi)$ and $R_{\text{off-diag}}(\phi)$ with numerical results for $(R_a)_{ij}$, obtained recently[44] for the ballistic Andreev interferometer of Fig. 13. This will show that the two-channel model accurately describes the ballistic limit. To emphasize that the two-channel model has a rather wide range of applicability, this interferometer, in contrast with that of Fig. 3(b), has been chosen to possess a normal region between the two superconductors. As a consequence, charge transport will take place both through Andreev reflection at the N-S interfaces, and through quasiparticle transmission.[47] Figures 14(a) and 14(b) show numerical results for the diagonal $(R_a)_{ii}$ and off-diagonal coefficients $(R_a)_{ij}$ $(i \neq j)$, respectively. Only of order N off-diagonal coefficients are non-negligible compared with unity, demonstrating that channels do indeed couple in

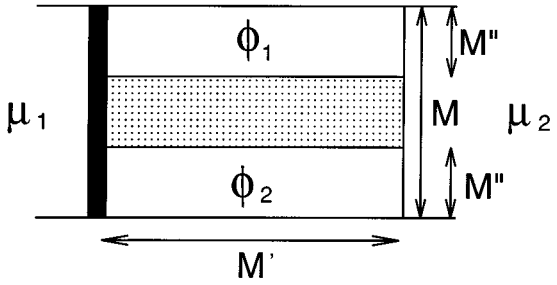

FIG. 13. Interferometer structure comprising two superconducting regions each of width M'' and separated by a distance M. The scattering region is connected to normal, external current carrying leads, of width $M + 2M''$. A normal barrier (shown black) is placed at the N-S interface. The current flows from left to right between external reservoirs with potentials μ_1 and μ_2. In the tight-binding model used in the numerical simulations, the barrier comprises a line of sites with diagonal elements $\epsilon_i = \epsilon_b$.

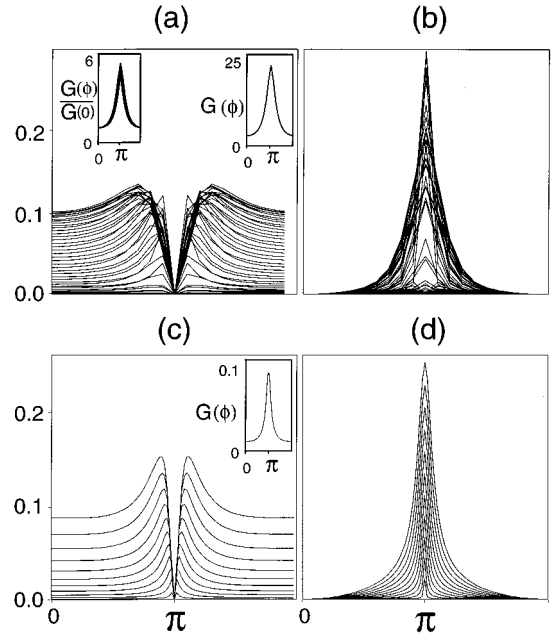

FIG. 14. (a) shows numerical results for the diagonal Andreev reflection coefficients $(R_a)_{ii}$ of the structure of Fig. 13, with $M=45$, $M'=50$, $M''=15$, $N=45$, and barrier potential, $\epsilon_b=2$. (b) shows corresponding results for the off-diagonal coefficients $(R_a)_{ij}$ with $i \neq j$. (c) and (d) show analytic results from a two channel calculation. The insets in the top right-hand corners of (a) and (c) show the corresponding conductances. The top left-hand inset of (a) shows plots of $G(\phi)/G(0)$ for five values of $N=35$, 40,45,50,55,60.

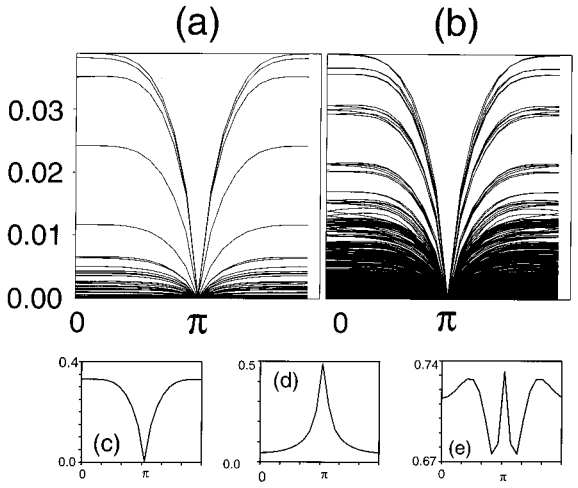

FIG. 15. Numerical results obtained from a tight-binding model of the structure of Fig. 13, but with the barrier replaced by a disordered region of length 30 sites. In these simulations, $M=45$, $M'=50$, $M''=15$, $N=45$, $\Delta_0=0.1$, and the disorder is $W=2.8$. (a) and (b) show results for diagonal and off-diagonal Andreev scattering coefficients, whose total contribution is shown in (c). (d) shows the behavior of the quasiparticle transmission, and (e) the total electrical conductance.

pairs. At $\phi=0$, there is no coupling between the channels and the scattering properties are those of N-independent channels, each with a barrier transmission coefficient T_i. The spectrum of the coefficients depends in detail on the shape of the barrier. The top right-hand inset of Fig. 14(a) shows the boundary conductance $G(\phi)$ obtained by summing the curves in Figs. 14(a) and 14(b), as well as the contribution due to normal transmission. Figures 14(c) and 14(d) show analytic results for $R_{\mathrm{dia}}(\phi)$ and $R_{\mathrm{off\text{-}diag}}(\phi)$ obtained from Eq. (16) by choosing ten pairs of transmission coefficients T_1, T_2, with $T_2=0.2T_1$. The inset of Fig. 14(c) shows the corresponding conductance obtained by summing the curves in Figs. 14(c) and 14(d).

Clearly the qualitative features of the exact simulation are reproduced by the two-channel analysis. Since the latter yields the N-channel conductance by summing over $N/2$ independent pairs of channels, the amplitude of oscillation, and hence the value at $\phi=\pi$, is predicted to scale with the number of open channels. This is confirmed by the exact numerical results shown in the top left-hand inset of Fig. 14(a), which shows plots of $G(\phi)/G(0)$ for five values of N ranging from $N=35$ to $N=60$.

Figures 11 and 12 demonstrate that when the resistance is dominated by tunnel barriers, the conductance-phase relation is insensitive to disorder and therefore a description of the ballistic limit is relevant. In the absence of tunnel barriers we now show that this insensitivity is no longer present. Figure 15 shows numerical results for the structure of Fig. 13, with $M=45$, $M'=50$, $M''=15$, but with the barrier replaced by a disordered normal region of length 30 sites. In the presence of disorder, the notion of diagonal and off-diagonal scattering is no longer useful, since channels corresponding to a given transverse component of the momentum, are no longer eigenstates. Instead they should be viewed as admixtures of eigenmodes of the normal-region transmission matrix. Diagonal and off-diagonal scattering are no longer distinct processes and therefore the scattering coefficients of Figs. 15(a) and 15(b) simply describe the same generic behavior. The sum of all the curves of Figs. 15(a) and 15(b) is the total contribution to the Andreev scattering coefficient, shown in Fig. 15(c). In this case, it appears that a theory describing average properties of a single channel, such as the quasi-one-dimensional description of quasiclassical theory, is indeed appropriate. For completeness, Fig. 15(d) shows the behavior of the quasiparticle transmission, and in Fig. 15(e) the conductance of Eq. (8). The peak at $\phi=\pi$ in the conductance appears to be due entirely to the normal transmission through the normal region, while the contribution due to Andreev scattering processes, at $\phi=\pi$, is completely suppressed. By reducing the width of the normal region between the two superconducting regions, as in the structure of Fig. 3(b), the contribution from the normal transmission will be eliminated, and the conductance at $\phi=\pi$ will vanish.

VII. DISCUSSION

In this paper, a detailed comparison between quasiclassical theory and numerical multiple-scattering calculations has been carried out. To ensure that the simulated structures fall within the parameter range where the approximations of quasiclassical Green-function methods hold, we have painstakingly examined each component of a given structure. For the N-I-S structures of Fig. 1, Fig. 2 shows that there is quantitative agreement between the two methods. For the interferometers of Fig. 3, there is broad qualitative agreement, although as shown in Figs. 9 and 4, some interesting differences are present.

In particular, the theory of Refs. 7–12 is a quasi-one-dimensional theory and for the symmetric structures of Fig. 3, necessarily predicts a vanishing conductance at $\phi=\pi$. This symmetry is not present at a microscopic level and therefore there is no such restriction on the results from an exact solution of the Bogoliubov-de Gennes equation. Figures 9(a), 9(b), and 9(c) suggest that for certain structures, this microscopic symmetry-breaking may be unimportant, but for other strengths of the tunnel barriers, Fig. 9(c) suggests that this artifact of one-dimensional implementations of quasiclassical theory will not be observed experimentally. In the quasiballistic limit, Figs. 11 and 12 show that although the overall conductance is increased, the qualitative shape of the conductance-phase curves can be unchanged. The ballistic limit can be described in terms of a two-channel model, which emphasizes the role of interchannel scattering as the origin of the finite value of the conductance at $\phi=\pi$. According to our results, this feature is almost insensitive to disorder, provided the resistance is dominated by tunnel barriers, as it is the case of Fig. 3(b). As a consequence, as already noted in Ref. 44, disorder is not a necessary feature of large amplitude Andreev interferometers. In the absence of tunnel barriers, this insensitivity to disorder is no longer present, and Fig. 15 shows that disorder does indeed change substantially the qualitative shape of the phase-dependent conductance.

Finally the above results demonstrate that quasiclassical theory yields the correct shape for the ensemble-averaged

conductance even down to extremely small system sizes. They also demonstrate that even without attempting a systematic extrapolation to a large number of channels, numerical multiple-scattering calculations on small structures, can yield results for ensemble-averaged properties of much larger systems.

ACKNOWLEDGMENTS

We would like to thank A. F. Volkov, A. D. Zaikin, and M. Leadbeater for extended discussions. Financial support from the EPSRC, the MOD, the Institute for Scientific Interchange, and NATO is also gratefully acknowledged.

[1] A. F. Andreev, Sov. Phys. JETP **19**, 1228 (1964).
[2] G. E. Blonder, M. Tinkham, and T. M. Klapwijk, Phys. Rev. B **25**, 4515 (1982).
[3] A. Kastalsky, A. W. Kleinsasser, L. H. Greene, F. P. Milliken, and J. P. Harbison, Phys. Rev. Lett. **67**, 3026 (1991).
[4] C. Nguyen, H. Kroemer, and E. L. Hu, Phys. Rev. Lett. **69**, 2847 (1992).
[5] P. Xiong, G. Xiao, and R. B. Laibowitz, Phys. Rev. Lett. **71**, 1907 (1993).
[6] S. J. Bakker, E. van der Drift, and T. M. Klapwijk, Phys. Rev. B **49**, 13 275 (1994).
[7] A. V. Zaitsev, JETP Lett. **51**, 41 (1990).
[8] A. F. Volkov and T. M. Klapwijk, Phys. Lett. A **168**, 217 (1992).
[9] A. F. Volkov, Phys. Lett. A **174**, 144 (1992).
[10] A. F. Volkov, A. V. Zaitzev, and T. M. Klapwijk, Physica C **210**, 21 (1993).
[11] Y. V. Nazarov, Phys. Rev. Lett. **73**, 1420 (1994).
[12] A. D. Zaikin, Physica B **203**, 255 (1994).
[13] F. W. J. Hekking and Y. V. Nazarov, Phys. Rev. Lett. **71**, 1625 (1993).
[14] F. W. J. Hekking and Y. V. Nazarov, Phys. Rev. B **71**, 6847 (1994).
[15] C. J. Lambert, J. Phys. Condens. Matter **3**, 6579 (1991).
[16] C. W. J. Beenakker, Phys. Rev. B **46**, 12 841 (1992).
[17] I. K. Marmorkos, C. W. J. Beenakker, and R. A. Jalabert, Phys. Rev. B **48**, 2811 (1993).
[18] C. W. J. Beenakker, Phys. Rev. B **47**, 15 763 (1993).
[19] C. W. J. Beenakker, B. Rejaei, and J. A. Melsen, Phys. Rev. Lett. **72**, 2470 (1994).
[20] B. Z. Spivak and D. E. Khmel'nitskii, JETP Lett. **35**, 413 (1982).
[21] B. L. Al'tshuler and B. Z. Spivak, Sov. Phys. JETP **65**, 343 (1987).
[22] C. J. Lambert, J. Phys. Condens. Matter **5**, 707 (1993).
[23] V. C. Hui and C. J. Lambert, Europhys. Lett. **23**, 203 (1993).
[24] A. V. Zaitsev, Phys. Lett. A **194**, 315 (1994).
[25] Y. Takane, J. Phys. Soc. Jpn. **63**, 2668 (1994).
[26] Y. V. Nazarov and T. H. Stoof, Phys. Rev. Lett. **76**, 823 (1996).
[27] J. Price (private communication).
[28] H. Pothier, S. Gueron, D. Esteve, and M. H. Devoret, Physica B **203**, 226 (1994).
[29] P. G. N. de Vegvar, T. A. Fulton, W. H. Mallison, and R. E. Miller, Phys. Rev. Lett. **73**, 1416 (1994).
[30] A. Dimoulas, J. P. Heida, B. J. v. Wees, and T. M. Klapwijk, Phys. Rev. Lett. **74**, 602 (1995).
[31] V. Petrashov, V. N. Antonov, P. Delsing, and T. Claeson, Phys. Rev. Lett. **74**, 5268 (1995).
[32] C. J. Lambert, V. C. Hui, and S. J. Robinson, J. Phys. Condens. Matter, **5**, 4187 (1993).
[33] V. C. Hui and C. J. Lambert, J. Phys. Condens. Matter **2**, 7303 (1990).
[34] C. J. Lambert and V. C. Hui, Physica B **165**, 1107 (1990).
[35] G. Eilenberger, Z. Phys. **214**, 195 (1968).
[36] K. D. Usadel, Phys. Rev. Lett. **25**, 507 (1970).
[37] G. M. Eliashberg, Sov. Phys. JETP **34**, 668 (1971).
[38] A. I. Larkin and Yu. N. Ovchinikov, Sov. Phys. JETP **41**, 960 (1976); **46**, 155 (1977).
[39] A. V. Zaitsev, Sov. Phys. JETP **59**, 863 (1984).
[40] M. Yu. Kuprianov and V. F. Lukichev, Sov. Phys. JETP **64**, 139 (1988).
[41] We recall that the matrix structure of $\hat{g}$ is due to the use of the nonequilibrium Keldysh formalism [L. V. Keldysh, Sov. Phys. JETP **20**, 1018 (1965)] and to allowance of anomalous propagators in the presence of superconductivity.
[42] H. Nakano and H. Takayanagi, Solid State Commun. **80**, 997 (1991).
[43] S. Takagi, Solid State Commun. **81**, 579 (1992).
[44] N. K. Allsopp, J. Sanchez-Canizares, R. Raimondi, and C. J. Lambert (unpublished).
[45] N. R. Claughton and C. J. Lambert, Phys. Rev. B **53**, 6605 (1996).
[46] N. R. Claughton and C. J. Lambert, Phys. Rev. B **51**, 11 635 (1995).
[47] The interferometer structure of Fig. 13 has been suggested in Ref. 44 with the purpose of showing that large amplitude conductance oscillations are indeed possible in the ballistic regime. The presence of a normal region between the two superconductors has been shown to optimize this effect.